2D parametric model for surface wave development under varying wind field in space and time

Vladimir Kudryavtsev, Maria Yurovskaya, Bertrand Chapron

JGR Oceans

RESEARCH ARTICLE
10.1029/2020JC016915

2D Parametric Model for Surface Wave Development Under Varying Wind Field in Space and Time

Vladimir Kudryavtsev[1,2], **Maria Yurovskaya**[2,1], **and Bertrand Chapron**[3,1]

[1]Russian State Hydrometeorological University, St. Petersburg, Russia, [2]Marine Hydrophysical Institute, Sebastopol, Russia, [3]Laboratoire d'Oceanographie Spatiale, Ifremer, Plouzane, France

This article is a companion to Kudryavtsev et al. (2021), https://doi.org/10.1029/2020JC016916.

Key Points:

- A fully consistent 2D parametric model of wave development under space-time varying winds is suggested
- The 2D model is based on first-principle conservation equations consistently constrained by self-similar fetch laws
- Coupled equations in characteristic form provide rapid assessments on how wave parameters are distributed under varying space-time wind forcing

Correspondence to:
V. Kudryavtsev,
kudr@rshu.ru

Citation:
Kudryavtsev, V., Yurovskaya, M., & Chapron, B. (2021). 2D parametric model for surface wave development under varying wind field in space and time. *Journal of Geophysical Research: Oceans*, *126*, e2020JC016915. https://doi.org/10.1029/2020JC016915

Received 24 OCT 2020
Accepted 13 MAR 2021

Abstract A fully consistent 2D parametric model of wave development under spatially and/or time varying winds is developed. Derived coupled equations are written in their characteristic form to provide practical means to rapidly assess how the energy, frequency and direction of dominant surface waves are developing and distributed under varying wind forcing conditions. For young waves, nonlinear interactions drive the peak frequency downshift, and the wind energy input and wave breaking dissipation are governing the wave energy evolution. With a prescribed wind wave growth rate, proportional to (u*/c) squared, wave breaking dissipation must follow a power-function of the dominant wave slope. For uniform wind conditions, this choice for the growth rate imposes solutions to follow fetch laws, with exponents $q = -1/4$, $p = 3/4$ correspondingly. This set of exponents recovers the Toba's laws, and imposes the wave breaking exponent equal to 3. A varying wind direction can then drive spectral peak direction changes, leading to the occurrence of focusing/defocusing wave groups over localized areas where wave-rays merge and cross. Significant (but finite) local variations of the energy are then expected under varying wind forcing. Propagating away from a stormy area, wave rays generally diverge, leading to dispersive swell systems. Examples of practical applications of this model are provided in (Kudryavtsev et al., 2021, companion paper).

Plain Language Summary A practical and rapid evaluation of wave conditions under stormy conditions is often required for navigation safety and coastal hazards. Surface waves and breakers are also essential components of the air-ocean coupled system to possibly control the dynamical evolution of extreme events. Here, a fully consistent 2D parametric model for wave development is solved in the storm frame of reference. Along wave-rays, peak energy and frequency evolve. Wave-rays can also bend under changes of the wind direction. The proposed method thus helps rapidly identify localized areas where wave-rays can merge or cross, leading to dangerous sea state hot spots. The suggested model will efficiently complement operational wave models, to simulate and map surface wave developments generated by moving tropical and extra-tropical cyclones.

1. Introduction

An efficient and ready-to-use statistical description of the surface gravity wavefield, especially its directional energy characteristics, is often needed for many engineering and scientific applications, in particular, for short-term forecasting of surface waves generated by Tropical Cyclones (TC). Full sophisticated spectral wave models certainly have the capability to provide detailed wave information. Moon et al., (2003) performed a comprehensive investigation of wind wavefield generated by TC Bonnie using WAVEWATCH III model (Tolman, 2009), buoy and aircraft Scanning Radar Altimeter (SRA) measurements. This study clearly demonstrated that using realistic wind forcing, the use of a high-resolution WAVEWATCH III model may yield successful simulations of surface wave fields in hurricane conditions.

Yet, computer limitations and/or needs to consider ensembles of solutions also invite to develop more simplified solutions. For instance, practical models can help to rapidly anticipate and document the role of partial resonance effects to increase the effective fetch and duration of the wave-growth process in the main direction of the tropical and extra-tropical weather systems, that is, the wave trapping phenomenon (e.g., Bowyer & MacAfee, 2005; Dysthe & Harbitz, 1987; King & Shemdin, 1978; Kudryavtsev, Golubkin, & Chapron, 2015; Young, 1988; Young & Vinoth, 2013). Indeed, despite the spatio-temporal complexity of extreme weather systems, generated surface waves are generally found to well follow

self-similar fetch laws, originally suggested by Kitaigorodskii (1962). For very intense low pressure systems, the main vortex structure of the winds apparently solely governs the spatial distribution of the waves and their associated directional characteristics. In that context, Wright et al., (2001) and more recently, Hwang and Fan (2017), Hwang and Walsh (2018), analyzed and quantified the azimuthal and radial distributions of wave spectra measured by airborne SRA inside TC. While the front half of the cyclone is well characterized by single wave systems, multiple wave systems are generally observed in the back and right quarters outside the radius of maximum wind. Hwang and Fan (2017), Hwang and Walsh (2018) further suggested an empirical model to describe the equivalent fetch and the dominant wave propagation direction.

For waves generated by varying wind field in both space and time, parametric models (e.g., Gunther, et al., 1979; Hasselmann, Sell, et al., 1976) should be more relevant. The parametric models simplify the evolution of the wave spectrum parameters: energy (significant wave height), frequency of the peak and its direction. The equations describing the evolution of relevant spectral moments are derived from the kinetic energy and momentum equations. Suggested by Hasselmann et al., (1976), the main principle of the parametric model construction is that the energy and momentum source terms can be specified to reproduce empirical fetch laws for idealized cases (i.e., constant wind forcing condition).

In this study, the main objective is to revise and pursue this heuristic approach, to propose the derivation of practical and fully consistent solutions for surface wave developments under spatially and temporally varying winds.

Section 2 describes the set of equations governing the evolution of wave energy, e, spectral peak frequency, ω_p, and its direction, φ_p. Equations derived through the energy and the momentum conservation equations are based on first principles. The main properties of these governing equations are:

- The evolution of the total energy is governed by wind energy input and dissipation. Nonlinear interactions implicitly appear via the spectral peak frequency downshift
- The peak frequency downshift is governed by the spectral gradient of the energy source around the peak, which is associated with nonlinear interactions when waves are young. When waves become developed, the rapid drop of wind forcing acts to restrain the peak frequency downshift
- The change of the spectral peak direction is driven by the energy input change from the veering wind

Section 3 specifies these driving sources in e, ω_p, and φ_p evolution equations. To that end, following a standard parametric model approach, these sources are first "calibrated" to match empirical fetch laws. They are then used to simulate waves evolution for a wind field varying in space and time. The key elements for the driving sources are the following:

- The wind input is proportional the square of the inverse wave age, the wave breaking dissipation is a power-function of the dominant wave steepness, and the rate of the frequency downshift is proportional to the dominant wave steepness to power 4
- For uniform wind conditions, self-similar solutions for energy and frequency development are conformed to Toba (1972)'s fetch law exponents. This set of exponents dictates that the energy dissipation must be proportional to the dominant wave steepness to power 6
- For the driving sources, proportionality constants are unambiguously linked with the pre-exponent constants of the fetch laws defined empirically, to complete the model development

Section 4 presents the final set of model equations written in the characteristic form, to describe the evolution of the wave parameters along the trajectory of wave-ray.

- Accounting for the 2D wind field variability results in the appearance of additional energy source caused by focusing/defocusing of wave-rays. This effect can lead to the formation of caustics zones where the energy is enhanced. Passing the caustic zone, wave-train trajectories further diverge, leading to wave attenuation away from the storm area
- Solution of the model equations by this method of characteristics provides practical means to rapidly map how the wave parameters are distributed along wave-train trajectories, and how multimodal surface

waves (mixed seas) are formed when wave-rays originating from different areas are crossing at a given space-time point

Section 5 provides illustrative model exemplars. Summary of the model and conclusions are given in Section 6. Application of the proposed 2D parametric model to simulate the surface wavefield under stationary and moving TC are presented in the companion paper.

2. Governing Equations

The parametric model considered here is limited to three main spectral parameters: energy, e, spectral peak frequency, ω_p, and its main direction φ_p, which are derivatives of the 0th—moments of the wave energy and momentum spectra. Hereinafter, we only consider deep water conditions, therefore wave frequency, ω, and wavenumber, k, are linked by the dispersion relation: $\omega^2 = gk$ where g is gravity acceleration, and interaction of the surface waves with the bottom is ignored. In this case, equations of conservation for the spectral density of the energy, $E(\omega,\varphi)$, and momentum, $M_i(\omega,\varphi)$ are (Hasselmann, Sell, et al., 1976; Phillips, 1977):

$$\partial E / \partial t + c_{gj}\partial E / \partial x_j = S^E \tag{1a}$$

$$\partial M_i / \partial t + c_{gj}\partial M_i / \partial x_j = S_i^M \tag{1b}$$

where c_{gj} is the group velocity, S^E and S_i^M the energy and momentum sources. The directional spectrum is represented as $E(\omega,\varphi) = A(\varphi - \varphi_p)F(\omega)$, where $A(\varphi - \varphi_p)$ the angular spreading, function satisfying condition $\int A d\varphi = 1$, and $F(\omega)$ is omnidirectional frequency spectrum. In the gravity range, the momentum spectrum $M_i(\omega,\varphi)$ is related to $E(\omega,\varphi)$ as: $M_i = k_i E / \omega = \kappa_i \omega E / g$ where κ_i is the unit wavenumber vector: $\kappa_i = [\cos\varphi, \sin\varphi]$. Correspondingly, the energy and the momentum total sources are linked as:

$$S_i^M = \kappa_i \omega S^E / g. \tag{2}$$

The energy source S^E is usually represented as the sum of the energy input from the wind (wind forcing), S_W, wave breaking dissipation, S_D, and the nonlinear four-wave interactions, S_N: $S^E = S_W - S_D + S_N$.

Wind forcing can generally be defined within the frame of the quasi-linear theory of wave generation as

$$S_W = \beta\omega A(\varphi - \varphi_p)F(\omega), \tag{3a}$$

where β is a growth rate specified here as (e.g., Plant, 1982)

$$\beta = c_\beta (u_* / c)^2 \cos^2(\varphi - \varphi_W) \tag{3b}$$

with $c_\beta = 4 \times 10^{-2}$, φ_W the wind direction, and u_* the air friction velocity linked to the wind speed at 10 m reference height, u_{10}, as: $u_* = c_D^{1/2} u_{10}$, where c_D is the sea surface drag coefficient. Relationship (Equation 3b) is only valid for waves traveling slower than the projection of the wind velocity on their directions. For $u_k \cos(\varphi - \varphi_W) - c < 0$, with u_k the wind speed at the height $z = k^{-1}$, the growth rate becomes negative, $\beta < 0$, that is, the wind input becomes an energy sink (see e.g., Merlink et al., 2003, and references cited therein). In the present study, we ignore negative values of β replacing them by zero, as:

$$\beta = c_\beta (u_* / c)^2 \cos^2(\varphi - \varphi_W) H_\beta(\varphi - \varphi_W, u_{10} / c) \tag{3c}$$

where H_β is a step-like (Heaviside type) function,

$$H_\beta\left(\varphi-\varphi_W, u_{10}/c\right)=\frac{1}{2}\left[1+\tanh\left(p\left(\cos\left(\varphi-\varphi_W\right)\frac{u_{10}}{c}-0.85\right)\right)\right] \tag{3d}$$

with p is a large number assigned here as $p=10$, and for sake of simplicity, we replace u_k by u_{10}.

Expression for the nonlinear interaction term S_N can be derived from first principles (Hasselmann, 1962; Zakharov, 2010). Exact calculations of S_N may be time consuming, and approximate schemes have been proposed (e.g., discrete interaction approximation [DIA], Hasselmann, et al., 1985, or its extension—the multiple DIA, Tolman, 2004, 2013).

Finally, a precise expression for the dissipation term is not known and different phenomenological approximations (e.g., model of dissipation due to wave capping by Hasselmann, 1974) are usually adopted for the wave development simulations.

However, a proper determination of the energy source, solution of the energy and momentum conservation equations must reproduce general semi-empirical properties of wave development expressed through the fetch-limited laws and shape of the wave spectrum. This is the general principle of the parametric model construction. Following this approach suggested by Hasselmann et al., (1976), the fetch-limited laws can indeed determine and constrain the energy and momentum source terms.

2.1. Energy

The integral of Equation 1a over all frequencies and directions provides the total energy, $e=\iint E d\varphi d\omega$, and the conservation equation writes:

$$\begin{aligned}\partial e/\partial t+\kappa_j^p\overline{c}_g\partial e/\partial x_j+e\partial\left(\kappa_j^p\overline{c}_g\right)/\partial x_j &= \iint S^E d\varphi d\omega\\ &\approx \iint\left(S_W-S_D\right)d\varphi d\omega\end{aligned} \tag{4}$$

where $\overline{c}_g$ is the mean group velocity weighted over the entire spectrum

$$\overline{c}_g=\int c_g F\left(\omega\right)d\omega/e, \tag{5}$$

and κ_j^p is unit vector of the spectral peak direction:

$$\kappa_j^p=\left[\cos\varphi_p,\sin\varphi_p\right]. \tag{6}$$

For the JONSWAP spectrum (D. Hasselmann, Ewing, & Dunckel, 1980), $\overline{c}_g$ can be evaluated, $\overline{c}_g=r_g c_{gp}$, with $r_g\simeq 0.9$, where c_{gp} is the group velocity of the spectral peak. After integration over ω and φ, contributions associated to source S_N cancel out, and the total energy is mainly governed by wind energy input and dissipation. This statement should not lead to the erroneous conclusion on a negligible role of nonlinear four-wave interactions for the wave energy evolution. Nonlinear interactions are essential. Nonlinear interactions implicitly appear to control the peak frequency downshift of the energy-containing part of the spectrum, subject to wind forcing and wave breaking dissipation (see below for more discussion).

2.2. Spectral Peak Kinematic

To describe the evolution of the spectral peak frequency and its direction, the momentum conservation equations are used (Gunther et al., 1981).

2.2.1. Frequency

Multiplying (Equation 1b) by κ_i and integrating the resulting equation over ω and φ, it follows:

$$\frac{\partial}{\partial t}\left(\overline{\omega}e\right)+\frac{\partial}{\partial x_j}\left(\kappa_j^p\overline{c}_g\overline{\omega}e\right)=g\iint\kappa_i S_i^M d\varphi d\omega \tag{7}$$

where $\overline{\omega}$ is the mean frequency weighted over the spectrum

$$\overline{\omega}=\int\omega F\left(\omega\right)d\omega\ /\ e \tag{8}$$

For the JONSWAP spectrum, $\overline{\omega}$ is related to the spectral peak frequency, ω_p, as $\overline{\omega}\approx 1.15\omega_p$. The ratio $\omega_p\ /\ \overline{\omega}$ is close to $\overline{c}_g\ /\ c_{gp}=r_g$ (about 5% difference), and for the sake of simplicity, we consider $\omega_p\ /\ \overline{\omega}=\overline{c}_g\ /\ c_{gp}=r_g$. This is already applied in Equation 7, where we replaced $\left(g\ /\ 2\overline{\omega}\right)$ by $\overline{c}_g$.

Equation 7, with use of Equation 4, leads to the following equation for the evolution of the peak frequency, ω_p:

$$\frac{\partial}{\partial t}\omega_p+\kappa_j^p\overline{c}_g\frac{\partial}{\partial x_j}\omega_p=\frac{r_g}{e}\int\left(\omega-\overline{\omega}\right)S_O^E d\omega \tag{9}$$

where $S_O^E\left(\omega\right)=\int S^E\left(\omega,\varphi\right)d\varphi$ represents the omnidirectional energy source. Expanding S_O^E into Taylor series $S_O^E\left(\omega\right)=S_O^E\left(\overline{\omega}\right)+\left(\partial S_O^E\ /\ \partial\omega\right)\left(\omega-\overline{\omega}\right)+\ldots$ the evolution of the peak frequency is thus governed by the derivative of S_O^E over ω in the vicinity of the spectral peak, that is, $\propto\left(\delta\omega\right)^3\partial S_O^E\ /\ \partial\omega$, where $\delta\omega$ relates to the spectral spread in the frequency domain. Since, under growing sea conditions, both wind forcing, S_W, and dissipation, S_D, have local extrema (maximum and minimum, correspondingly) in the peak vicinity, $\omega=\overline{\omega}$, the main mechanism leading to spectral peak downshifts is thus S_N. Indeed, S_N exhibits a strong spectral gradient in this peak spectral area (see e.g., Figure 4b in K. Hasselmann, Sell, et al., 1976 for illustration). Under growing sea conditions, the balance of wind forcing and dissipation provides energy gain to the dominant waves, see Equation 4, but downshifts of their frequency peaks are driven by nonlinear four-wave interactions which redistribute the energy between wave components.

However, when developing waves approach the fully developed conditions, i.e., when the inverse wave age, $\alpha=u_{10}\ /\ c_p$, is $\alpha\rightarrow 0.85$, the wind energy input (Equation 3a) decreases. Around the peak, the gradient of the total source, $\partial S_O^E\ /\ \partial\omega$, becomes more strongly affected by this wind energy input decay. The gradient of S_W is positive, in contrast to S_N, and acts to restrain the spectral peak downshift when waves are approaching a fully developed stage.

2.2.2. Direction

For the evolution of the spectral peak direction, the momentum Equation 1b is first integrated over ω and φ, leading to

$$\frac{\partial}{\partial t}\left(\kappa_i^p\overline{\omega}e\right)+\frac{\partial}{\partial x_j}\left(\kappa_i^p\kappa_j^p\overline{c}_g\overline{\omega}e\right)=g\iint S_i^M d\varphi d\omega \tag{10}$$

Then, using Equations 7 and 2, we have

$$\frac{\partial}{\partial t}\varphi_p+\kappa_j^p\overline{c}_g\frac{\partial}{\partial x_j}\varphi_p=\frac{1}{\overline{\omega}e}\iint\sin\left(\varphi-\varphi_p\right)\omega S^E d\varphi d\omega \tag{11a}$$

where the total energy term S^E is a sum of wind energy input, wave breaking dissipation and nonlinear wave-wave interactions: $S^E=S_W-S_D+S_N$. Balance of these terms under integral in the right hand side (r.h.s. hereinafter) of Equation 11a governs the spectral peak direction change.

The directional spreading of wave energy, $A\left(\varphi-\varphi_p\right)$ is further assumed to be much narrower than the angular distribution of the wind wave growth rate (Equation 3c). Up to second order on the angular width of the wave spectrum, the integral in r.h.s. of Equation 11a can be evaluated as

$$\begin{aligned}\iint \sin\left(\varphi-\varphi_p\right)\omega S^E d\varphi d\omega &\simeq \iint \omega\left[\left(\beta_p E - S_D + S_N\right)\Delta\varphi + \beta_p' E\Delta\varphi^2\right]d\varphi d\omega \\ &\simeq \beta_p' \iint \omega E\Delta\varphi^2 d\varphi d\omega\end{aligned} \tag{11b}$$

where $\Delta\varphi = \varphi - \varphi_p$ is the deviation from the mean wave direction, β' indicates derivative of β over the azimuth, and subscript "p" indicates that growth rate and its derivative are fixed at the peak direction, $\varphi = \varphi_p$. Source terms associated to dissipation, S_D, and nonlinear four-wave interactions, S_N, are functions (or functional) of the wave spectrum E. Therefore, first angular moments of the wind energy input in direction of the spectral peak, $\beta_p E$, S_D and S_N (terms enclosed in parentheses inside the square brackets in Equation 11b) must thus vanish. Hence, changes of the peak wave direction are mostly impacted by veering wind conditions through deviation of the maximum of the wind wave growth rate from the wave peak direction.

Then, substituting (Equation 3c) into the r.h.s. of Equation 11a with Equation 11b, we obtain the following:

$$\frac{\partial}{\partial t}\varphi_p + \kappa_j^p \overline{c}_g \frac{\partial}{\partial x_j}\varphi_p = -C_\varphi \alpha^2 \omega_p H_p \sin\left[2\left(\varphi_p - \varphi_W\right)\right] \tag{12}$$

where H_p is the step-like function (Equation 3d) applied for the spectral peak parameters, and C_φ relates to spectral moments:

$$C_\varphi = c_D c_\beta \delta\varphi^2 \frac{\int \omega^4 F\left(\omega\right)d\omega}{\omega_p^3 \int \omega F\left(\omega\right)d\omega} \tag{13}$$

where c_D is the drag coefficient, and $\delta\varphi^2$ is the variance of the angular spread of wave energy: $\delta\varphi^2 = \int\left(\varphi-\varphi_p\right)^2 A\left(\varphi-\varphi_p\right)d\varphi$, equal to $\delta\varphi^2 = 0.16$ for the JONSWAP-type spectrum. To note, in Equation 13, the integral in numerator of the fraction can be divergent, if all wave spectral components are integrated (with the upper limit as $\propto \ln\omega$). Therefore, to evaluate C_φ, it can be suggested to restrict the spectral domain integration to $\overline{\omega} - \delta\omega < \omega < \overline{\omega} + \delta\omega$. In this case numerically evaluated using the JONSWAP spectrum, the fraction in Equation 13 is about 1.4.

Equation 12 can be compared with previously suggested semi-empirical and numerical models of the spectral peak direction evolution (Gunther et al., 1981; Holthuijsen et al., 1987; van Vledder & Holthuijsen, 1993; Young et al., 1987 and references cited therein). In such kind of models, r.h.s. of Equation 12 is written in a relaxation approximation as: $-\sin\left(\varphi_p - \varphi_w\right) / T_R$, where T_R is a relaxation time-scale evaluated semi-empirically as:

$$1 / T_R = c_r\left(g / u_{10}\right)\alpha^r \tag{14}$$

where r is an exponent, and c_r is an empirical constant. For $r = 2$, c_r is reported to vary from $c_r = 5.3\times10^{-5}$ to $c_r = 1.4\times10^{-4}$, and for $r = 1$, c_r varies from $c_r = 6\times10^{-5}$ to $c_r = 1.2\times10^{-4}$ [see Table 3 from van Vledder & Holthuijsen, 1993, and references cited therein for r and c_r].

Under our proposed development, r.h.s. of Equation 12 written in terms of the relaxation approximation reads: $1 / T_R = 2C_\varphi\left(g / u_{10}\right)\alpha^3$, where the factor 2 takes into account the angle change in the sinus function in Equation 12. Notice, since the growth rate is vanishing at $\alpha \to 0.85$ (via Heaviside-function H_p in Equation 12), the inverse relaxation time tends to zero, $u_{10} / \left(gT_R\right) \to 0$, for waves approaching their fully developed stage. The dependency of T_R on wave age is stronger than experimentally reported, power exponent 3 against 2 or 1. But the model proportionality coefficient equals to $c_r \equiv 2C_\varphi = 3.6\times10^{-5}$ (at $c_\beta = 4\times10^{-2}$ and $c_D = 2\times10^{-3}$), and provides consistency with reported empirical estimates of T_R in the range of wave

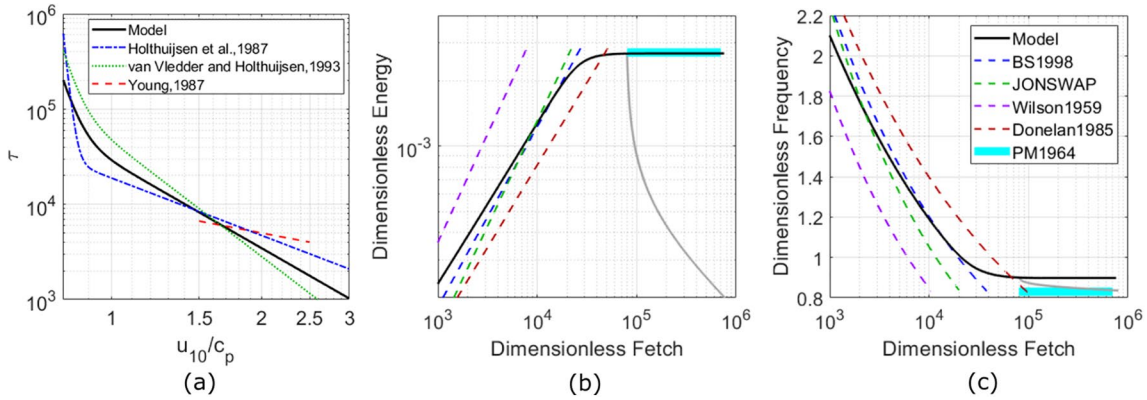

Figure 1. (a) Dimensionless relaxation time, $\tau \equiv T_r g / u_{10}$, of wave direction turning as a function of inverse wave age. (b) Dimensionless energy and (c) peak frequency versus dimensionless fetch. Line notations are given in legend (see also corresponding place in the paper for more details). Gray lines in plots (b) and (c) show model evolution of dimensionless energy and frequency after the wind suddenly dropped at fetch $\tilde{x} = 8 \times 10^4$. In this case dimensionless energy and frequency are scaled by the same wind speed as at $\tilde{x} < 8 \times 10^4$.

age $\alpha = 1 \div 3$. It should also be noticed, that wave age exponent "3" in the model T_R is a consequence of the adopted expression (Equation 3c) for the wave growth rate. If an "alternative" expression for the growth rate is chosen, for example, $\propto u_* / c_p$, then the model exponent turns into "2".

Van Vledder and Holthuijsen (1993) also reported results of numerical simulations of time evolution of the wave direction under sudden and rotating wind direction changes, using EXACT-NL model (S. Hasselmann and Hasselmann, 1985). Model simulations were performed for the cases when the spectral peak frequency was less than twice the Pierson-Moskowitz frequency, $\alpha_{PM} = 0.83$. Parameterization of the model simulations in terms of semi-empirical relationship (Equation 14) gave: $c_r = 2.2 \times 10^{-5}$ and $r = 4$, attenuating to zero if $\alpha \to \alpha_{PM}$. Dependence of $1/T_R$ on wave age, predicted by EXACT-NL, is a bit stronger than in the present model (4 against 3). However, $u_{10}/(gT_R)$ in both models tends to zero for fully developed waves, and magnitudes of $u_{10}/(gT_R)$ for double Pierson-Moskowitz frequency, $\alpha = 2\alpha_{PM}$ are the same (1.67×10^{-4} against 1.65×10^{-4} for present model). Some difference between the model relaxation times at "large" α (say at $\alpha > 3\alpha_{PM}$) is not important, since T_R of such waves is smaller than the wind variability time-scale. In this case, direction of developing waves for all models simply follows the veering wind direction.

Comparison of the model relaxation time with numerical simulations using EXACT-NL model presented in (van Vledder & Holthuijsen, 1993; Young et al., 1987) and with semi-empirical model by Holthuijsen et al., (1987) is shown in Figure 1a. Referring to this figure, one may conclude that the present model is consistent with both the robust numerical simulations and empirical data.

3. Input Sources: Link to Self-Similarity

Except for the wave direction, Equation 12, the source terms for the conservation equations for the energy (Equation 4) and frequency (Equation 9) are not defined. Following K. Hasselmann et al., (1976), fetch-limited laws can be used to "calibrate" these source terms, that is, to reproduce wind-wave development characteristics for stationary wind conditions (see e.g., review in Badulin at al., 2007):

$$\tilde{\omega}_p \equiv \alpha = c_\alpha \tilde{x}^q, \tilde{e} = c_e \tilde{x}^p \tag{15a}$$

where $\tilde{x} = xg / u^2$ is the dimensionless fetch, u is the wind speed (e.g., wind speed at 10 m height), g is the gravity acceleration, $\tilde{\omega}_p = \omega_p u / g$ and $\tilde{e} = eg^2 / u^4$ are dimensionless spectral peak frequency and energy. These self-similar laws (Equation 15a) can be represented as one-parametric expression to linking the dimensionless energy and the wave age

$$\tilde{e} = c_e\left(\alpha / c_\alpha\right)^{p/q} \tag{15b}$$

3.1. Energy

The input energy source in Equation 4 is defined as

$$\iint\left(S_W - S_D\right)d\varphi d\omega = I_w - D \tag{16}$$

where $I_W$is the integral wind energy input which using Equation 3c is

$$I_W = r_W c_\beta\left(u_* / c_p\right)^2\cos^2\left(\varphi_p - \varphi_W\right)H_p\omega_p e \tag{17}$$

with $r_W = \int\omega^3 F d\omega / \left(\omega_p^3 e\right)$, evaluated to $r_W = 2.35$, for a JONSWAP spectrum. The integral dissipation D in Equation 16 is expressed by considering a nonlinear attenuation based on a threshold steepness criterion:

$$D = \omega_p e\left(k_p^2 e / \varepsilon_T^2\right)^n \tag{18}$$

where k_p is the spectral peak wavenumber, ε_T is a threshold steepness, n defines the nonlinear attenuation. For fetch-limited and uniform wind conditions, we can suggest the integral dissipation to be proportional to the integral wind input, that is, $D / I_w = \gamma$ where $\gamma < 1$ is a constant. Integral dissipation and inverse wave age are then linked: $(k_p^2 e)^n \propto \alpha^2$. Using fetch laws (Equation 15a), the dissipation exponent can then be defined from the exponents of the fetch laws:

$$n = \frac{2q}{p + 4q} \tag{19}$$

For the case of fetch-wave development, Equation 4 then becomes:

$$\partial\left(\overline{c}_g e\right) / \partial x = r_W c_\beta c_D\left(1 - \gamma\right)\left(g / u\right)\alpha^3 e \tag{20}$$

and reorganized using fetch laws (Equation 15) as

$$\begin{aligned}\partial\ln\left(e / \alpha\right) / \partial\tilde{x} &= 2b\alpha^4 \\ &= 2bc_\alpha^4\tilde{x}^{4q}\end{aligned} \tag{21}$$

With $b = (r_W / r_g)\left(1 - \gamma\right)c_\beta c_D$. Equation 21 will provide fetch law-type solutions, only if the fetch law exponent q in the r.h.s. of Equation 21 equals to

$$q = -1 / 4 \tag{22}$$

Notice, that this value is linked to the wind input source term (Equation 17), where $\beta \propto \left(u_* / c_p\right)^2$. Adopting another parametrization for the growth rate in Equation 3b, for example, $\beta \propto u_* / c_p$ (Snyder et al., 1981) or $\beta \propto \left(u_* / c_p\right)^{4/3}$ (Pushkarev & Zakharov, 2015), the exponent of α in the r.h.s. of Equation 21 becomes "3" or "10/3", leading to the fetch law exponents $q = -1/3$ or $q = -0.3$, correspondingly. These values are certainly acceptable, and have been used in previous parametric models (Fontaine, 2013; Hasselmann, Sell, et al., 1976). Also worth mentioning the model by Guan and Sun (2004) where energy sources I_W and D are similar to Equations 17 and 18, with n fixed a priory at $n = 2$. Postulating the 3/2-power law by Toba (1972), the authors also arrive at (Equation 22), and as a consequence of the Toba's law, at$p = 3/4$. Thus, the fetch law exponents and dissipation power in the model by (Guan & Sun, 2004) are consistent with relationship (Equation 19).

Keeping $q = -1/4$, that is, growth rate Equation 3b, the constant b in Equation 21 is also linked to the fetch law parameters as

$$b = \frac{1}{2}(p-q)c_\alpha^{-4} \tag{23}$$

Given r_W, r_g, c_β, c_D, combined in a single constant $C_e = (r_W / r_g)c_\beta c_D$, the proportionality constant γ can then be derived:

$$(1-\gamma) = 1/2 \times (p-q)c_\alpha^{-4}C_e^{-1}. \tag{24}$$

Subsequently, the threshold steepness, ϵ_T^2, is deduced from $\gamma = \left(k_p^2 e / \epsilon_T^2\right)^n / \left(C_e \alpha^2\right)$, and using Equation 15b, expressed as

$$\varepsilon_T^2 = \frac{c_e c_\alpha^{-p/q}}{(\gamma C_e)^{1/n}} \tag{25}$$

with γ defined by 24. The integral source term, I_w–D, in the energy conservation Equation 4, calibrated on fetch law pre-exponent constants c_e and c_α via 25, finally reads:

$$\begin{aligned} I_w - D &= \omega_p e\left(\tilde{I}_w - \tilde{D}\right) \\ \tilde{I}_w - \tilde{D} &= C_e H_p \alpha^2 \cos^2(\varphi_p - \varphi_W) - \left(e k_p^2 / \varepsilon_T^2\right)^n \end{aligned} \tag{26}$$

where we recall, $C_e = (r_W / r_g)c_\beta c_D$ absorbs growth rate constant, c_β, and the drag coefficient, c_D. To note, when $\alpha \cos(\varphi_p - \varphi_W) < 0.85$ is locally fulfilled, the wind energy input is switched off, and waves turn into a regime of swell and attenuate under dissipation.

3.2. Peak Frequency

3.2.1. Effect of Non-Linear Interactions

As discussed in Section 2.2.1, during the active stage of wave development, the waves are young, and non-linear four-wave interactions control the peak frequency downshift. In the frequency conservation Equation 9, the input source term can be estimated as

$$\begin{aligned} e^{-1}\int(\omega-\bar{\omega})S_O^N d\omega &\approx e^{-1}\partial S_O^N / \partial\omega \int(\omega-\bar{\omega})^2 d\omega \\ &\propto -e^{-1}\delta\omega^2 \langle S_O^N \rangle \\ &\propto -\omega_p^2 k_p^4 e^2 \propto -g^{-4}\omega_p^{10} e^2 \end{aligned} \tag{27}$$

where $\delta\omega \propto \omega_p$ is a spectral frequency width. Taking into account scale of the non-linear interaction $\langle S_O^N \rangle$ is cubic with wave energy, the derivative of S_O^N over ω is evaluated as $\partial S_O^N / \partial\omega \propto \langle S_O^N \rangle / \delta\omega$ (e.g., Badulin & Zakharov, 2017; Zakharov, 2010). Equation 9 with Equation 27 for fetch-limited conditions then reads

$$c_{gp}\partial\omega_p / \partial x \propto -g^{-4}\omega_p^{10} e^2 \tag{28}$$

Substituting parameters derived from fetch laws (Equation 15), the so-called "magic" universal relationship between fetch law exponents is recovered (Badulin & Zakharov, 2017; Zakharov, 2010):

$$2p + 10q + 1 = 0 \tag{29}$$

Since q is already prescribed, $q = -1/4$ (to satisfy the energy balance equation), the relationship dictates the exponent for the energy equal to

$$p = 3/4 \tag{30}$$

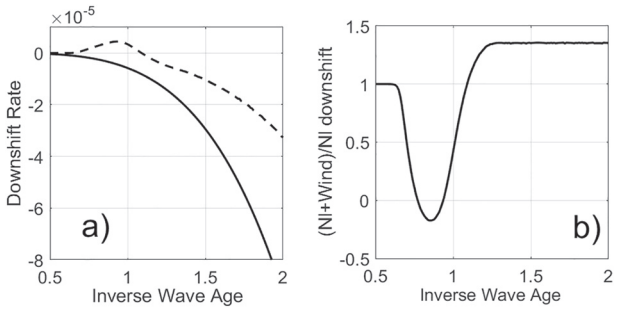

Figure 2. (a) Peak frequency downshift due to (solid line) nonlinear interaction according to (Equation 31), and (dash line) due to wind forcing predicted by Equation 32 with Equation 33. (b) Ratio of consolidate shift (nonlinear interactions plus wind forcing) to nonlinear downshift.

This set of exponents, $q = -1/4$ and $p = 3/4$, gives $H_s \propto T_p^{3/4}$ (where H_s is wave height and T_p is the peak period) that corresponds to fetch laws suggested by Toba (1972). These exponents further determine the exponent n for the wave breaking dissipation (Equation 18), and according to Equation 19 it becomes $n = 2$.

Substituting Equation 15 in Equation 28, the proportionality constant in Equation 28 is derived, leading to:

$$\begin{aligned} e^{-1}\int\left(\omega-\bar{\omega}\right)S_O^N d\omega &= C_\alpha g^{-4}\omega_p^{10}e^2 \\ &= C_\alpha\omega_p^2\left(k_p^2 e\right)^2 \end{aligned} \tag{31}$$

With C_α absorbing the fetch law parameters: $C_\alpha = 1/2\times qc_\alpha^{-10}c_e^{-2}$, and the downshift of the spectral peak frequency is proportional to the wave energy to power 2 (or proportional to the slope of the spectral peak waves to power 4).

While nonlinear four-wave interactions are governing this peak frequency downshift, an alternative view can also be hypothesized. In random rough seas, the dominant waves occur in groups. At the centers of these groups, waves can exceed a critical steepness leading to breaking events. Suggested by Tulin (1996), breaking events can then contribute to local spectral peak downshifts [see also Fontaine, 2013 for more references and discussion]. According to Tulin (1996), the peak downshift rate is proportional to D/e. In the present development $D/e \propto \left(k_p^2 e\right)^2$, and Equation 31 is consistent with Tulin's hypothesis. Though the underlying physics is different, four-wave interactions or wave breaking dissipation, wave group occurrence link these processes. Indeed, Longuet-Higgins (1969) pointed out that most of the nonlinear energy transfer occurs among groups. This can explain the resulting Equation 31 governing the spectral peak downshift to be formally equivalent for both processes.

3.2.2. Effect of Wind Input

As already discussed in Section 2.2.1, the nonlinear interactions govern the peak frequency downshift as long as the waves are young. When waves approach the fully developed conditions, $\alpha\cos\left(\varphi_p-\varphi_W\right)\to 0.85$, the wind energy input (Equation 3a with Equation 3c) rapidly decays, to impact the gradient of the energy source around the peak, $\partial S_O^E/\partial\omega$, and thus, according to Equation 9, the peak frequency downshift. The rate of peak downshift associated to the wind forcing writes

$$\partial\omega_p/\partial t = e^{-1}\int\int_{\bar{\omega}-\delta\omega}^{\bar{\omega}-\delta\omega}\left(\omega-\bar{\omega}\right)S_O^W d\omega \tag{32}$$

With S_O^W the omnidirectional wind source term. This rate is shown in Figure 2 along with the downshift rate due to four-wave interactions (Equation 31). For young sea, the wind forcing weakly contributes to peak downshift of young waves. For waves approaching full development, $\alpha\to 0.85$, the wind forcing starts to significantly act against the downshift driven by nonlinear four-wave interactions. Near $\alpha\approx 0.85$, the magnitudes of nonlinear and wind induced downshift rates are comparable, but with opposite signs. This leads to decelerate the peak downshift, leveling off the peak frequency.

For $\alpha < 0.85$, the wind forcing could lead to "upshift" the spectral peak. The wind energy input vanishes in the vicinity of the spectral peak, and taking into account the attenuation due to dissipation, the spectral peak shape can be deformed and shift toward higher frequencies, more subject to wind forcing.

To take this effect into account, a bell-shaped function,

$$\Delta_p = 1-1.25\times sech^2\left[10\left(\alpha_p-0.85\right)\right],$$

simulating right plot in Figure 1 (with $\alpha_p = \cos\left(\varphi_p - \varphi_W\right)u_{10} / c_p$), is introduced in Equation 31 to largely reduce the peak downshift if the wave peak phase velocity approaches the wind velocity, and to upshift the peak frequency if the wind energy input locally vanishes. This function corresponds to the derivative of the step-like function 3d, used to limit the wind energy input for fully developed waves. The r.h.s. of the peak frequency conservation (Equation 9) finally writes:

$$e^{-1}\int\left(\omega - \overline{\omega}\right)S_O^E d\omega = r_g C_\alpha \Delta_p \omega_p^2 \left(k_p^2 e\right)^2 \tag{33}$$

4. Model Equations: Ray Characteristic Form

The set of the model equations are developed in their characteristic form. Under spatially and time varying winds, solutions of this set of equations by the method of characteristics provide effective numerical means to rapidly calculate and map how the energy, frequency and direction of dominant surface waves are distributed along characteristics (wave-train trajectories or rays), and how a field of multimodal surface waves (mixed seas) can form if trajectories of wave trains originating from different regions cross at a given point in space and time.

Equation 4 with Equation 26 can be expressed in ray characteristic form as:

$$\frac{de}{dt} = -e\left(\partial\overline{c}_g / \partial l + \overline{c}_g \partial\varphi_p / \partial n\right) + \omega_p e\left(\tilde{I}_w - \tilde{D}\right) \tag{34}$$

where $d / dt = \partial / \partial t + \kappa_j^p \overline{c}_g \partial / \partial x_j$ is the total derivative for wave train traveling along the ray described by

$$\frac{d}{dt}x_j = \kappa_j^p \overline{c}_g \tag{35}$$

where we remind that $\overline{c}_g$ is the mean group velocity linked the group velocity of the spectral peak as $\overline{c}_g = r_g c_{gp}$.

4.1. Divergence of Group Velocities

The first term in the r.h.s of Equation 34 corresponds to the divergence of the group velocity, $\partial\left(\kappa_j^p \overline{c}_g\right) / \partial x_j$, written in local orthogonal coordinates, where l and n are directed along and normal to the ray trajectory, correspondingly. Divergence of wave rays is an inherent feature of waves driven by a varying 2D wind field, and also for swell traveling away from the storm area. In the latter case, far from the storm area, the divergence of swell rays provides classical attenuation of wave energy proportional to inverse distance to the storm area.

Along-ray and cross-ray components of the group velocity divergence are

$$\partial\overline{c}_g / \partial l \approx \Delta\overline{c}_g / \left(\overline{c}_g \Delta t\right) = \overline{c}_g^{-1} d\overline{c}_g / dt \tag{36}$$

$$\overline{c}_g \partial\varphi_p / \partial n \simeq \overline{c}_g \Delta\varphi_p / \Delta n, \tag{37}$$

where $\Delta\varphi_p$ is the difference between neighbor characteristics separated by the small distance Δn, evolving in time as

$$d\Delta n / dt = \Delta\varphi_p \overline{c}_g \tag{38}$$

Equation for $\Delta\varphi_p$ follows from Equation 12, and reads

$$\frac{d}{dt}\Delta\varphi_p = -T^{-1}\left[\left(\Delta\varphi_p - \Delta\varphi_w\right) + \frac{\Delta u}{u}\tan\left(2\left(\varphi_p - \varphi_W\right)\right)\right] \tag{39}$$

with T is a relaxation time scale defined as

$$T^{-1} = 2C_\varphi H_p \alpha^2 \omega_p \cos\left(2\left(\varphi_p - \varphi_W\right)\right), \tag{40}$$

$\Delta\varphi_W$ and Δu are the wind direction and speed differences between neighbor characteristics. Developing young seas are almost aligned with the wind, $\varphi_p \approx \varphi_w$. Then ignoring the impact of wind speed difference, second term in the square brackets of r.h.s of Equation 39, we obtain

$$\begin{aligned}\frac{d}{dt}\Delta\varphi_p + T^{-1}\Delta\varphi_p &= T^{-1}\Delta\varphi_w \\ &= T^{-1}G_W^n\Delta n\end{aligned} \tag{41}$$

where $G_W^n = \Delta\varphi_w / \Delta n$ is the cross-ray component of the wind direction gradient. Solution of the coupled system, Equation 38 and Equation 41, can further be combined.

Defining the cross-ray gradient of wave direction, $G_n = \Delta\varphi_p / \Delta n$, which takes into account the cross-ray divergence of group velocities, the energy balance Equation 34 now becomes:

$$\frac{d}{dt}\ln\left(\overline{c}_g e\right) = -\overline{c}_g G_n + \omega_p\left(\tilde{I}_w - \tilde{D}\right) \tag{42}$$

Note, the coupled Equations 38 and 41 can also be combined to describe the evolutions of the cross-ray gradient:

$$dG_n / dt + G_n / T + \overline{c}_g G_n^2 = G_W^n / T \tag{43}$$

4.2. Caustic Formation

Integrating Equation 38, the distance between neighbor characteristics, Δn, evolves in time as

$$\Delta n = \Delta n_0 + \int_{t_0}^{t} \overline{c}_g \Delta\varphi_p dt \tag{44}$$

where Δn_0 is an initial distance.

When wave-ray diverge, that is, $\Delta\varphi_p > 0$, the wave-ray "width" Δn grows in time, and since term $G_n = \Delta\varphi_p / \Delta n$ in Equation 42 is positive, it leads to an energy decrease. For the freely propagating waves (swell), the relaxation time scale T defined by Equation 40 is infinitely large and following Equation 41, $\Delta\varphi_p$ keeps a constant value along the ray. In this case, solution of Equation 42, ignoring impact of dissipation, is: $e \propto 1 / t$, that provides classical attenuation of wave train energy as inverse travel time, or as inverse distance r, (since $t = r / \overline{c}_g$) from the storm area where swell originated.

When wave-ray converge, that is, $\Delta\varphi_p < 0$, Δn may vanish at some location. In this case, the term $G_n = \Delta\varphi_p / \Delta n$ tends to infinity, and Equation 42 loses its validity. This phenomenon corresponds to the formation of a "caustic point." In this development, such a singularity is a direct consequence of the assumption that a wave group is almost monochromatic. In nature, wave trains have a finite spectral bandwidth. It leads to group velocity variations, with a standard deviation, Δc_g, defined as

$$\left(\Delta c_g\right)^2 = \int\left(c - \overline{c}_g\right)^2 F\left(\omega\right)d\omega \,/\, \int F\left(\omega\right)d\omega \tag{45}$$

with integrals taken over all the frequencies. For the JONSWAP spectrum, Δc_g scaled by the mean group velocity is $\left(\Delta c_g \,/\, \overline{c}_g\right)^2 = 4.6\times10^{-2}$. Dominant waves can then be represented by a superposition of elementary monochromatic beams. At a given time, positions of elementary waves, as well as their contribution to the total cross-ray divergence, are distributed along the ray, around the mean position $l = \overline{c}_g t$ and within the interval $\Delta l \,/\, l = \pm\Delta c_g \,/\, \overline{c}_g$. The overall impact of these superposed wave beams on the mean cross-ray group velocity divergence is discussed in Appendix 1. For the cross-ray gradient of the waves directions, $G_n = \Delta\varphi_p \,/\, \Delta n$, the averaged contribution of these elementary waves reads:

$$G_n = \frac{\Delta\varphi_p}{\Delta n_0}\left[\frac{\Delta n \,/\, \Delta n_0}{\left(\Delta n \,/\, \Delta n_0\right)^2 + \left(1 \,/\, 2\cdot\Delta c_g \,/\, \overline{c}_g\right)^2}\right] \tag{46}$$

where $\Delta\varphi_p$ and Δn are solutions of the equations system (Equation 41 and Equation 38).

Thus, divergence/convergence of wave-rays, described by the first term in the r.h.s of Equation 42, can remarkably impact the wave energy balance, leading to attenuation/enhancement of the local wave energy. As demonstrated below, in Section 5, for wind waves under development and young, this impact can effectively be suppressed by wave breaking dissipation that constrains the energy level. However, when waves become "free," turning into a swell regime, focusing/defocusing effects play important role to affect the energy level. In this context, it is worth to emphasize that converging wave-rays passing the caustic zone, inevitably become divergent. Thus, the overall effect of convergence/divergence of wave-rays generated by 2D wavefield is this divergence property in the storm far zone, resulting in radial attenuation of the energy with distance from the storm.

4.3. Final Set of Model Equations

Assembling the different equations written in the characteristic form, the final closed system of differential equations becomes:

$$\frac{d}{dt}\ln\left(\overline{c}_g e\right) = -\overline{c}_g G_n + \omega_p\left(\tilde{I}_w - \tilde{D}\right) \tag{47}$$

$$\frac{d}{dt}c_{gp} = -\frac{r_g C_\alpha}{2}\Delta_p g\left(k_p^2 e\right)^2 \tag{48}$$

$$\frac{d}{dt}\varphi_p = -C_\varphi\alpha^2\omega_p H_p \sin\left[2\left(\varphi_p - \varphi_W\right)\right] \tag{49}$$

$$\frac{d}{dt}x_j = \kappa_j^p\overline{c}_g \tag{50}$$

where the cross-ray divergence factor G_n, and dimensionless rate of wind input-minus-dissipation $\tilde{I}_w - \tilde{D}$ in Equation 47 are defined by Equation 46 and 26 correspondingly; the peak frequency conservation Equation 48 is expressed in terms of the spectral peak group velocity, $c_{gp} = g \,/\, \left(2\omega_p\right)$. The mean group velocity appearing in Equations 47 and 50 is linked to c_{gp} as: $\overline{c}_g = r_g c_{gp}$ with $r_g \simeq 0.9$.

As established, this coupled system describes the development of surface waves under a varying wind field in both space and time, as well as the evolution of swell propagation when the wind forcing is switched off.

This system can further be supplemented with a relationship describing the breaking of the dominant waves. In terms of the total length of breaking crests, L, the energy dissipation is (Phillips, 1985)

$$D = bg^{-1}c^5L \tag{51}$$

with b in the range $b = 10^{-4} \div 10^{-2}$. In the present model development, the dissipation is defined by Equation 18, leading to the following relation for the length of breaking crests of dominant waves:

$$L_p = b^{-1}\varepsilon_T^2 k_p \left(ek_p^2 / \varepsilon_T^2\right)^3 \tag{52}$$

Correspondingly, the fraction of sea surface covered by peak wave breakers, the whitecap coverage, $Q_p = \epsilon k_p^{-1} L_p$, with $\epsilon \ll 1$, can be evaluated

$$Q_p = c_Q \left(ek_p^2 / \varepsilon_T^2\right)^3 \tag{53}$$

where $c_Q = b^{-1}\epsilon_T^2\epsilon$ is absorbing the other constants. Whitecap coverage is proportional to the peak wave steepness to power "6." For developing waves, $ek_p^2 \propto \alpha$ and $Q_p \propto \alpha^3$, hence the younger the waves the larger is the fraction of the surface covered by whitecaps. If the peak frequency is fixed, the whitecap coverage becomes proportional to the wind speed to power "3," as often reported (see e.g., Brumer et al., 2017, and references cited therein). If the fetch is fixed, $\alpha \propto \left(xg / u^2\right)^{-1/4}$, the whitecap coverage is proportional to the wind speed to power "3/2."

Note, breakers from the equilibrium range of wind waves likely provide the major part of the whitecap coverage, Q_e, which is least dependent (if dependent at all) on wave age and mostly driven by the wind (Phillips, 1985). The total whitecap coverage thus corresponds to the sum $Q = Q_p + Q_e$, and this spatial distribution is both wind speed and wave-age dependent. Yet, the largest thickness of foam layers is more likely associated with dominant wave breakers (Reul & Chapron, 2003). Emitted radiations from thick foam-induced brightness temperature will generally rise and impact low-frequency microwave measurements, especially under extreme conditions (e.g., Reul, Chapron, et al., 2017). For these intense and varying wind conditions, the distributed thickness of foam layers is then expected to be strongly wave-age dependent.

4.4. Model Parameters/Constants

Overall, there is only one parameter—the wind wave growth rate parameter, that influences the driving sources for the energy, peak frequency and direction evolutions. In the present study, the growth rate is adopted in form Equation 3. For this choice, solutions of the model equations for wave development at limited fetch and uniform wind conditions, have self-similar form Equation 15a with exponents $q = -1/4$ and $p = 3/4$. This set of exponents via Equation 19 prescribes the power exponent $n = 2$ in wave breaking dissipation (Equation 18), which is an important resulting model parameter. Fit of any empirical data on wave development at fetch limited conditions by Equation 15a with $q = -1/4$ and $p = 3/4$, provides values of the model pre-exponent constants c_α and c_e. These two constants together with drag coefficient c_D, and growth rate constant c_β, are the only "tuning" model constants which define the driving source constants in the evolution Equations 47–50. Once defined, the driving source constants can then be used to simulate wave evolution under a wind field varying in space and time.

Transition of developing waves to developed ones is regulated by a "threshold" inverse wave age value 0.85 in the growth rate (Equation 3c) and in the bell-function, Δ_p, in Equation 33. This value introduces native ending of wind energy input to waves and a limit for the peak frequency downshift, leading to the appearance of fully developed wind waves.

A summary of the model constants is given in Appendix 2.

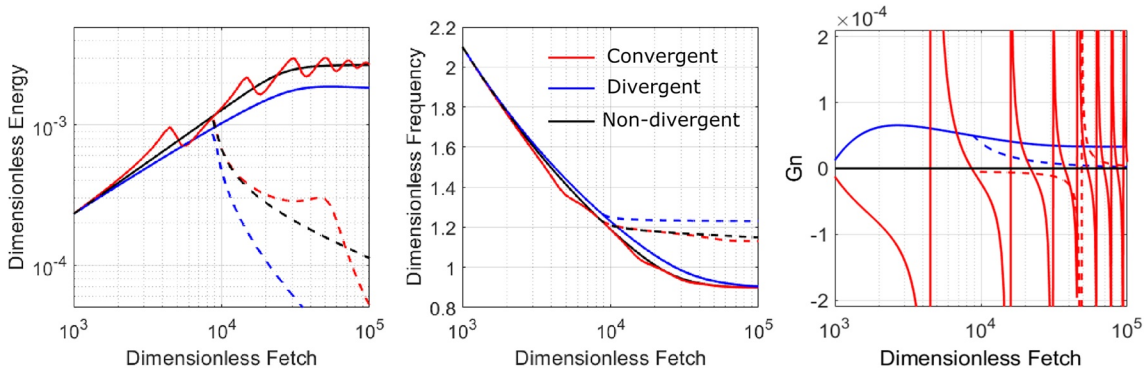

Figure 3. Fetch-limited development of (a) energy, (b) peak frequency, and (c) cross-ray gradient, Equation 46 for (black lines) nondivergent, (blue lines) divergent, and (red lines) convergent off-shore wind field. Dash lines of different colors show model parameters for the case when wind speed is abruptly vanished at dimensionless fetch $\tilde{x} = 0.9 \times 10^4$, and the solid lines show the case when wind filed is continuous.

5. Model Exemplars

5.1. Uniform Wind: Recovering Fetch Laws

An example of the model performance for a fetch-limited wave development is shown Figures 1b and 1c. For reference, the empirical dependencies of the dimensionless energy and wave age on fetch suggested by Hasselmann et al., (1973), Donelan et al., (1985), Babanin and Soloviev (1998), and Wilson (1965) are also shown. At early stage of development, the model reproduces these empirical dependencies, in accord with the definition of the model input source terms calibrated on fetch laws reported by Babanin and Soloviev (1998) (see Appendix 2 for more details). More importantly, the model provides a smooth transition from developing to fully developed waves. This corresponds to the decay of the wind energy input that restrains both the energy growth and the peak frequency downshift. The model energy level saturates at $eg^2 / u_{10}^4 = 2.7 \times 10^{-3}$, which corresponds to the Pierson and Moskowitz (1964) limit, a bit lower than the revisiting value suggested by Alves et al., (2003). The model peak frequency saturates at $\omega_p u_{10} / g = 0.9$, that, in turn, is a bit higher than limits suggested either by Pierson-Moskowitz (1964) and Alves et al., (2003). However, if waves are fully developed and wind "suddenly" drops out, as in Figure 1 at fetch $\tilde{x} = 8 \times 10^4$, the nonlinear interactions continue to shift the frequency peak, ω_p, toward lower values, close to the Pierson and Moskowitz limit 0.83. In this case the restraining action associated to the spectral gradient of the wind forcing vanishes, and the downshift results from the energy transfer associated to nonlinear wave interactions. Strongly dependent on the wave steepness, the significant decrease of the dominant wave energy then contributes to level off the peak downshift.

Following the present development, it is worth to note that the evolution of the swell system is also self-similar, that is, the evolution is described by the same dimensionless functions of dimensionless space and time variables. The rate of swell energy attenuation is then found much larger than predicted by Badulin and Zakharov (2017) under the weakly turbulent theory, which predicts an energy decrease $\propto x^{-1/12}$.

5.2. Effect of Wind Velocity Divergence/Convergence

Next, we consider the case of a fetch-limited wave development under the action of a wind, uniform in the main direction, but varying in the perpendicular direction. As a prototype, a roll-like structure of the wind field is suggested: the wind velocity component of the main flow, u_{10}, is constant, and the orthogonal component, v, only varies in the y-direction. It is also assumed that $v \ll u_{10}$. This orthogonal component produces convergent/divergent zones which are aligned with the main flow.

Figure 3 illustrates the expected effects of wind divergence/convergence on the development of the waves. The magnitude of the gradient of wind direction G_W is specified here as $|G_W| = 10^{-4}$ rad/m, negative or positive in the divergence or convergence zones, respectively. Small wind direction changes gradually rotate the

dominant waves. The divergence of the wind velocity forces the wave rays to widen. In turn, this widening effect results in cross-ray divergence of group velocities, Figure 3, leading to an additional energy sink in the energy balance equation (first term in the r.h.s. in Equation 42). For developing waves, this impact is not crucial: an overall energy decrease of about 30%, and subsequent deceleration of the frequency downshift, Figure 3. Ray-divergence effect on the swell is more remarkable, with a rapid attenuation of the energy and shorter peak wavelength away from the wind front, as compared with the reference nondivergent wind, Figure 3.

Convergent wind field results in more complicated wave development. The wind velocity convergence forces wave rays to progressively concentrate. This inevitably leads to the formation of caustic, where the wave energy locally accumulates. Away from this ray-crossing area, wave-rays widen to become again subject to convergent wind forcing, and the formation of another (new) caustic zone, Figure 3c. This process is recurrent, resulting in the modulation of wave energy along the wave development, as well expressed in Figure 3a. Wave energy modulations cause modulations for the spectral peak frequency, but of second-order in the present case, Figure 3b.

If the wind abruptly drops, the impacts of wind forcing on wave direction changes and wave-ray thickening is terminated. In the course of their evolutions, swell trains will then keep memory on the rate of ray thickness widening/narrowing which is constant in time and in space. In the specific case shown in Figure 3, the swell leaves with a decreasing ray width. It then approaches a caustic zone at distance around $\tilde{x} = 5 \times 10^4$, where the energy largely increases, almost by factor 2 when compared to the reference run. Away from the caustic zone, swell rays diverge, and the energy rapidly attenuates, due to this additional cross-ray divergence of the group velocities.

6. Summary and Conclusion

A fully consistent 2D parametric model of development of the surface waves parameters (significant wave height, peak frequency and direction) under spatially and temporally varying winds is suggested. The 2D model is based on first-principle conservation equations of the energy and the momentum, consistently constrained by self-similar fetch laws (Equation 15). The model consists of coupled equations written in the characteristic form, which describe time evolution of wave-trains energy, Equation 47, group velocity, Equation 48, and direction, Equation 49, along wave-rays described by Equation 50. Following the main principle of the parametric model construction, the energy and the group velocity source terms are tuned to reproduce empirical 1D self-similar fetch laws for idealized case of constant wind velocity (Hasselmann, Sell, et al., 1976).

The wind energy input and wave breaking dissipation are the governing sources of the wave energy evolution. Considering the wind wave growth rate to be $\propto \left(u_* / c\right)^2$, Equation 3, the wave breaking dissipation becomes a power-function of the dominant wave steepness, Equation 18. It is suggested that under uniform wind conditions, wave breaking dissipation of developing waves is proportional to the wind energy input. In this case, solution of the energy balance Equation 47 in the fetch law variables (15) exists if exponent q in Equation 15a is equal to $q = -1/4$. The wave breaking dissipation exponent n in Equation 18 is then linked to the fetch law exponents by relationship 19. The energy source provides growth of the wave energy while waves are young and developing. If wind velocity locally drops or/and changes direction, the wind forcing is reduced, and the dissipation leads to the energy attenuation, providing smooth transition of wavefield from wind driven seas to swell.

Nonlinear interactions are essential to drive the spectral peak frequency downshift. In terms of peak group velocity, its growth is proportional to the peak wave steepness to power 4, Equation 48. Under uniform wind field condition, solution of this equation in fetch law variables (Equation 15) requires fulfillment of the magic relationship (Equation 29) between the energy and frequency exponents, as found by Badulin and Zakharov (2017) and Zakharov (2010). Since q is already defined, $q = -1/4$, the fetch exponent for the energy must be $p = 3/4$, conforming with Toba (1972)'s relationships. This set of fetch law exponents imposes the power $n = 2$ in the wave breaking dissipation (Equation 18).

The nonlinear interactions govern the peak frequency downshift as long as the waves are young. When the peak phase velocity approaches wind velocity, the wind energy input to the waves rapidly decays and acts against the downshift driven by nonlinear four-wave interactions. Near inverse wave age $\alpha \approx 1$, the magnitudes of nonlinear and wind-induced downshift rates are comparable, but with opposite signs. This leads to the leveling off the peak frequency and appearance of so called the "fully-developed" seas.

It is important to emphasize that it is the parametrization of the growth rate in form Equation 3, that is, as $\propto \left(u_* / c\right)^2$, which leads to the fetch laws type solutions (Equation 15) with the exponents $q = -1/4$ and $p = 3/4$, that, in turn, also prescribes exponent $n = 2$ in wave breaking dissipation (Equation 18). If an alternative parametrization of the growth rate is chosen, for example, as a linear function of u_*/c, this ultimately leads to another set of the exponents: $q = -1/3$, $p = 7/6$, and $n = 4$. Such fetch law exponents are also plausible (see e.g., review by Badulin & Zakharov, 2017), and may potentially be adopted in the model. However, the present model utilizes the wind wave growth rate in form Equation 3 which was comprehensively grounded either theoretically and experimentally.

Final tuning of the model is to determine proportionality constants in the energy, Equation 47, and peak group velocity, Equation 48, evolution equations. These constants are unambiguously linked with the pre-exponent constants in the fetch laws (15) (known empirically) with predefined $q = -1/4$, $p = 3/4$, and their determination complete the tuning of 2D parametric model.

Under veering wind conditions, neither dissipation nor nonlinear interactions are capable (by themselves) to change direction of the spectral peak waves. The wind forcing, via its deviation of the growth rate maximum, coinciding with wind direction, from the spectral peak direction, is the source to drive wave direction change, and its rate is fully defined by magnitude and the azimuthal dependence of the wind growth rate, that is, no extra tuning of the model is needed.

Varying in space winds can then lead to the occurrence of focusing/defocusing wave groups to affect the energy balance. The focusing of wave-rays leads to the possible formation of caustics over areas where wave-rays merge and cross. Formally, the energy balance equation loses its validity with solutions tending to infinity. However, dominant waves in nature have a finite spectral spread and random phases. Caustic locations for the different spectral beams, forming the spectrum of dominant waves, are thus randomly scattered in space. This precludes fully singular behavior, and solutions are found to predict significant (but finite) enhancements of the energy over the focusing caustic zones. Further propagating, wave rays diverge, leading to wave attenuation away from the storm area (Ardhuin et al., 2009; Delpey et al., 2010; Munk et al., 1963; Snodgrass et al., 1966).

Under spatially and time varying winds, this 2D parametric model can thus provide practical means to rapidly map and assess how the energy (significant wave height), frequency and direction of dominant surface waves are distributed. Full sophisticated spectral wave models certainly have these capabilities, as for example, demonstrated by Moon et al., (2003). Yet, the proposed simplified 2D parametric model offer very fast wave ray-characteristic solutions, to accommodate for both rapid ensemble evaluations and sensibility studies to model wind adjustments (e.g., Hell et al., 2019). Applications can also serve to provide prior-information to analyze high-resolution satellite remote sensing measurements (e.g., Kudryavtsev, Golubkin, & Chapron, 2015; Kudryavtsev, Yurovskaya, et al., 2017; Mouche et al., 2019; Quilfen et al., 2018).

Within the storm generated area, the proposed model also provides relationships to assess the varying breaking distribution of the dominant waves. For intense and varying wind conditions, the distributed thickness of foam layers is then expected to be spatially varying and strongly wave-age dependent. This may have practical applications to improve the interpretation of emitted radiations from thick foam-induced brightness temperatures to low-frequency microwave measurements, especially under extreme conditions (e.g., Reul, Chapron, et al., 2017; Reul, Tenerelli, et al., 2012).

Further methodological improvements may certainly be foreseen. In particular, the validation of the main features and properties of directional swell systems that outrun their generating strong wind areas can presently benefit from the combined data collected by extensive in situ buoy and remote sensing measurements (e.g., Collard et al., 2009), including the recently launched China-France Ocean Satellite (CFOSAT) SWIM

instrument (Aouf et al., 2021; Hauser et al., 2020) and Copernicus Sentinel-1A and -B SAR measurements. From more systematic comprehensive study of swell fields and the present development, directional peak wave properties may be improved, and possibly more directly parameterized based on the storm structure and intensity, translation and rotation. Such an effort can help improve the physics of numerical wave models and has applications to remote sensing algorithm developments.

Application of the proposed 2D parametric model to simulate the surface wavefield under stationary and moving TC are presented in the companion paper (Kudryavtsev et al., 2021).

Appendix 1: Effect Spectral Width on Caustic

Let us assume that the wavefield is represented by superposition of elementary monochromatic beams with the mean group velocity, $\overline{c}_g$, and standard deviation, Δc_g, relative to the mean value defined by Equation 45. Elementary waves at a given time t, as well as their contributions to cross-ray divergence, are distributed along the ray around the mean position $l = \overline{c}_g t$ within the interval $\Delta l / l = \pm \Delta c_g / \overline{c}_g$.

To take into account the integrated impact of these wave beams on cross-ray group velocity divergence, the evolution is considered over small space-time scales, much smaller than scales of the wave development. From Equation 38 at $\Delta\varphi_p = \text{const}$, the wave beam width varies as $\Delta n = \Delta n_0 + \Delta\varphi_p l$, where $\Delta n_0 = \Delta n(0)$, and $l = c_g t$. Consequently, cross-ray gradient, $G_n = \Delta\varphi_p / \Delta n$, for an elementary beam reads:

$$\begin{aligned} G_n &= G_{n0} / \left[1 + G_{n0} l\right] \\ &= 1 / \left(l - l_c\right) \end{aligned} \tag{A1.1}$$

where $G_{n0} = \Delta\varphi_p / \Delta n_0$, and $l_c = -1/G_{n0}$ is the caustic location for a beam. Notice that A1.1 is also a solution of equation of 43 on time scales of evolution which are much less than the relaxation time T.

For the sake of simplicity, a Gaussian distribution relative to the mean value, $\overline{c}_g$, is considered. Using the JONSWAP spectrum, the standard deviation (std) of this Gaussian distribution, Δc_g, can be evaluated. Relative to the carrying wave position, $\overline{l}$, the positions of the elementary waves then also obey a Gaussian distribution:

$$P(\delta l) = 1 / \left(\sqrt{\pi}\Delta l\right) \exp\left(-\delta l^2 / \Delta l^2\right) \tag{A1.2}$$

where $\delta l = l - \overline{l}$, and Δl is std of positions defined as $\Delta l = \left(\Delta c_g / \overline{c}_g\right) l_c$. The mean value of (A.1.1) averaged overall wave beams, $\overline{G}_n$, at a point $\overline{l} = \overline{l}(t)$ on the ray is:

$$\begin{aligned} \overline{G}_n\left(\overline{l}\right) &= \int_{-\infty}^{+\infty} G_n(l) P\left(l - \overline{l}\right) dl \\ G_n(l) &= 1 / \left(l - l_c\right) \end{aligned} \tag{A1.3}$$

Figure A1 shows estimated mean cross-ray gradients of ray directions. Taking into account the finite spectral width of the wave groups removes asymptotic singularities for the energy focusing in the vicinity of a caustic point, originally predicted by A1.1.

In practice, integral (A1.3) can be approximated by the expression

$$\begin{aligned} G_n / G_{n0} &= -\frac{l / l_c - 1}{\left(l / l_c - 1\right)^2 + \left(1/2 \cdot \Delta c_g / c_g\right)^2} \\ &= \frac{\Delta n / \Delta n_0}{\left(\Delta n / \Delta n_0\right)^2 + \left(1/2 \cdot \Delta c_g / c_g\right)^2} \end{aligned} \tag{A1.4}$$

A modified expression for the cross-ray gradient of ray directions, uniformly valid everywhere including caustic zones, can thus be suggested

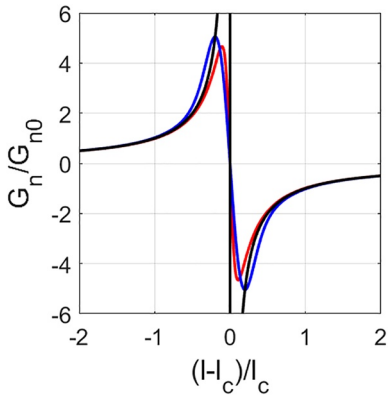

Figure A1. Cross-ray gradient of wave directions around the caustic point $l = l_c$ for: (black line) monochromatic wave, relation (A1.1); (blue line) wave packet with Gaussian distribution of group velocities, relation (A1.3); (red line) approximate relation (A1.5).

$$G_n = \frac{\Delta\varphi_p}{\Delta n_0}\left[\frac{\Delta n \,/\, \Delta n_0}{\left(\Delta n \,/\, \Delta n_0\right)^2 + \left(1/2\cdot \Delta c_g \,/\, \overline{c}_g\right)^2}\right] \tag{A1.5}$$

where $\Delta\varphi_p$ and Δn are solutions of Equations 41 and 38, correspondingly, with $\Delta c_g \,/\, \overline{c}_g = 0.21$ the group velocity std scaled by the mean value.

Appendix 2: Choice of Model Constants

In this section we summarize the key model constants. The growth rate constant, c_β, in Equation 3b varies in the range $c_\beta = \left(2 \div 6\right)\times 10^{-2}$ (Plant, 1982), and in the present study it is fixed at $c_\beta = 4\times 10^{-2}$. In the range from moderate to high winds, the surface drag coefficient, c_D, is described by known empirical relationships. There are much more uncertainties for c_D at high winds, above 20 m/s, and a conventional agreement is to consider c_D to saturate around $c_D = 2\times 10^{-3}$. Targeting simulation of the waves under TC, we adopt this value, and suggest to use it at any wind speeds, including moderate one.

The fetch law exponents p and q in Equation 15a are already prescribed in the model as$p = 3/4$, and $q = -1/4$. To specify the pre-exponent constants c_α and c_e, we, follow recommendations formulated in (Badulin et al., 2007) and adopt empirical laws suggested by Babanin and Soloviev (1998). The empirical fetch exponents reported by Babanin and Soloviev (1998) are: $q = -0.275$, $p/q = -3.01$, which are different from the model one: $q = -1/4$, $p/q = -3$. Therefore, to get the best fit to Babanin and Soloviev (1998) data, we specify c_α and c_e in our model as:

$$c_\alpha = 11.8 \; and \; c_e = 1.3\times 10^{-6}. \tag{A2.1}$$

Correspondingly, the dissipation exponent n is

$$n = \frac{2q}{p+4q} = 2 \tag{A2.2}$$

At assigned $c_\beta = 4\times 10^{-2}$ and $c_D = 2\times 10^{-3}$, and the fitted pre-exponent values (A2.1), the dimensionless "wind-input-minus-dissipation", parameter $\left(1-\gamma\right)$, becomes

$$\left(1-\gamma\right) = \left(p-q\right)c_\alpha^{-4} \,/\, \left(2rc_\beta c_D\right) = 0.12, \tag{A2.3}$$

and the threshold steepness in dissipation (Equation 18) is

$$\varepsilon_T^2 = \frac{c_e c_\alpha^{-p/q}}{\left(\gamma c_\beta c_D\right)^{1/n}} = 0.15 \tag{A2.4}$$

Remarkably, if we express ϵ_T^2 via steepness $\epsilon_T^2 = a^2k^2/2$, this value appears consistent with the vertical acceleration at the crest approaching −g/2 and a limiting Stokes-wave steepness, *ak*, equal to 0.5.

Finally, the model constants in the driving sources for the energy, Equation 47 with Equation 26 and the peak frequency, Equation 48, evolution, are defined as

$$C_e = \left(r_W / r_g\right) c_\beta c_D = 2.2 \times 10^{-4} \tag{A2.5}$$

$$C_\alpha = 1/2 \times q c_\alpha^{-10} c_e^{-2} = -1.4 \tag{A2.6}$$

Constant C_φ, necessary for the evolution of the spectral peak direction, Equation 49, is evaluated with an angular spreading $\delta\varphi^2 = 0.16$ (typical for JONSWAP spectrum) and the integral spectral bandwidth taken in the range $\bar{\omega} - \delta\omega < \omega < \bar{\omega} + \delta\omega$ ($\delta\omega$ is the standard deviation of JONSWAP spectrum frequency spreading), to give

$$C_\varphi = c_\beta c_D \delta\varphi^2 \frac{\int \omega^4 F(\omega) d\omega}{\omega_p^3 \int \omega F(\omega) d\omega} = 1.8 \times 10^{-5} \tag{A2.7}$$

All the model constants are summarized in Table 1.

Table 1
Summary of the Model Constants

Constant	Value	Number of equation (where it appears)	Comment
c_D	2e−3	13	Drag coefficient
c_β	4e−2	11b	Growth rate constant
p	¾	15a, 15b	Fetch low exponent for energy
q	−1/4	15a, 15b, 22	Fetch low exponent for frequency
n	2	18	Exponent for wave breaking dissipation
c_α	11.8	15a, 15b	Fetch-low constant for frequency
c_e	1.3e−6	15a, 15b	Fetch-low constant for energy
γ	0.88	20, 24	Dissipation over wind input ratio,
ε_T^2	0.15	18, 25	Threshold squared steepness for wave breaking dissipation
$\delta\varphi^2$	0.16	13	Angular spread of wave energy
r_g	0.87	8, 17, 20, 24, 25	$\bar{c}_g / c_{gp}, \omega_p / \bar{\omega}$
r_w	2.35	17, 20, 24, 25, 48	$\int \omega^3 F d\omega / \left(\omega_p{}^3 e\right)$
C_e	2.16e−4	26	Constant in energy evolution equation
C_a	−1.41	31, 48	Constant in group velocity evolution equation
C_φ	1.8e−5	13, 49	Constant in peak direction evolution equation

Data Availability Statement

The empirical data on the wind wave development used in this analysis (Section 2.1 and Section 5.1) are available through (van Vledder & Holthuijsen, [1993]; Young et al., [1987]; Holthuijsen et al., [1987]; Hasselmann et al., [1973]; Babanin & Soloviev, [1998]).

Acknowledgments
The core support for this work was provided by the Russian Science Foundation through the Project № 17-77-30019 at RSHU. The support of the Ministry of Science and Education of the Russian Federation under State Assignment No. 0555-2021-0004 at MHI RAS, and State Assignment No. 0763-2020-0005 at RSHU are gratefully acknowledged. Part of this study is a contribution to ESA MAXSS project C.N.4000132954/20/I-NB.

References

Alves, J. H. G. M., Banner, M. L., & Young, I. R. (2003). Revisiting the Pierson-Moskowitz asymptotic limits for fully developed wind waves. *Journal of Physical Oceanography*, *33*(7), 1301–1323. https://doi.org/10.1175/1520-0485(2003)033<1301:rtpalf>2.0.co;2

Aouf, L., Hauser, D., Chapron, B., Toffoli, A., Tourrain, C., & Peureux, C. (2021). New directional wave satellite observations: Toward improved wave forecasts and climate description in Southern Ocean. *Geophysical Research Letters*, *48*, e2020GL091187. https://doi.org/10.1029/2020gl091187

Ardhuin, F., Chapron, B., & Collard, F. (2009). Observation of swell dissipation across oceans. *Geophysical Research Letters*, *36*, L06607. https://doi.org/10.1029/2008GL037030

Babanin, A. V., & Soloviev, Y. P. (1998). Field investigation of transformation of the wind wave frequency spectrum with fetch and the stage of development. *Journal of Physical Oceanography*, *28*, 563–576. https://doi.org/10.1175/1520-0485(1998)028<0563:fiotot>2.0.co;2

Badulin, S. I., Babanin, A. V., Zakharov, V. E., & Resio, D. (2007). Weakly turbulent laws of wind-wave growth. *Journal of Fluid Mechanics*, *591*, 339–378. https://doi.org/10.1017/S0022112007008282

Badulin, S. I., & Zakharov, V. E. (2017). Ocean swell within the kinetic equation for water waves. *Nonlinear Processes in Geophysics*, *24*, 237–253. https://doi.org/10.5194/npg-24-237-2017

Bowyer, P. J., & MacAfee, A. W. (2005). The theory of trapped-fetch waves with tropical cyclones–An operational perspective. *Weather and Forecasting*, *20*, 229–244. https://doi.org/10.1175/WAF849.1

Brumer, S. E., Zappa, C. J., Brooks, I. M., Tamura, H., Brown, S. M., Blomquist, B. W., et al. (2017). Whitecap coverage dependence on wind and wave statistics as observed during SO GasEx and HiWinGS. *Journal of Physical Oceanography*, *47*(9), 2211–2235. https://doi.org/10.1175/jpo-d-17-0005.1

Collard, F., Ardhuin, F., & Chapron, B. (2009). Monitoring and analysis of ocean swell fields from space: New methods for routine observations. *Journal of Geophysical Research*, *114*, C07023. https://doi.org/10.1029/2008JC005215

Delpey, M. T., Ardhuin, F., Collard, F., & Chapron, B. (2010). Space-time structure of long ocean swell fields. *Journal of Geophysical Research*, *115*, C12037. https://doi.org/10.1029/2009JC005885

Donelan, M., Hamilton, J., & Hui, W. (1985). Directional spectra of wind-generated oceanwaves. *Philosophical Transactions of the Royal Society Mathematical, Physical and Engineering Sciences*, *315*(1534), 509–562.

Dysthe, K. B., & Harbitz, A. (1987). Big waves from polar lows? *Tellus A: Dynamic Meteorology and Oceanography*, *39A*, 500–508. https://doi.org/10.1111/j.1600-0870.1987.tb00324.x

Fontaine, E. (2013). A theoretical explanation of the fetch- and duration-limited laws. *Journal of Physical Oceanography*, *43*(2), 233–247. https://doi.org/10.1175/JPO-D-11-0190.1

Guan, C., & Sun, J. (2004). Similarities of some wind input and dissipation source terms. *China Ocean Engineering*, *18*(4), 629–642.

Günther, H., Rosenthal, W., & Dunckel, M. (1981). The response of surface gravity waves to changing wind direction. *Journal of Physical Oceanography*, *11*, 718–728. https://doi.org/10.1175/1520-0485(1981)011<0718:trosgw>2.0.co;2

Gunther, H., Rosenthal, W., Weare, T. J., Worthington, B. A., Hasselmann, K., & Ewing, J. A. (1979). A hybrid parametrical wave prediction model. *Journal of Geophysical Research*, *84*(C9), 5727. https://doi.org/10.1029/jc084ic09p05727

Hasselmann, D. E., Ewing, M. J. A., & Dunckel, M. (1980). Directional wave spectra observed during JONSWAP 1973. *Journal of Physical Oceanography*, *10*, 1264–1280. https://doi.org/10.1175/1520-0485(1980)010<1264:dwsodj>2.0.co;2

Hasselmann, K. (1962). On the non-linear energy transfer in a gravity-wave spectrum Part 1. General theory. *Journal of Fluid Mechanics*, *12*, 481–500. https://doi.org/10.1017/s0022112062000373

Hasselmann, K. (1974). On the spectral dissipation of ocean waves due to white capping. *Boundary-Layer Meteorology*, *6*, 107–127. https://doi.org/10.1007/bf00232479

Hasselmann, K., Barnett, T. P., Bouws, E., Carlson, H., Cartwright, D. E., Enke, K., et al. (1973). Measurement of wind wave growth and swell decay during the Joint North Sea Wave Project (JONSWAP). *Deutschen Hydrographischen Zeitschrift*, *12*, 95.

Hasselmann, K., Sell, W., Ross, D. B., & Müller, P. (1976). A parametric wave prediction model. *Journal of Physical Oceanography*, *6*, 200–228. https://doi.org/10.1175/1520-0485(1976)006<0200:APWPM>2.0.CO;2

Hasselmann, S., & Hasselmann, K. (1985). The Wave Model EXACT-NL. In *Ocean wave modeling*. Springer. https://doi.org/10.1007/978-1-4757-6055-2_24

Hasselmann, S., Hasselmann, K., Allender, J. H., & Barnett, T. P. (1985). Computations and Parameterizations of the nonlinear energy transfer in a gravity-wave Specturm. Part II: Parameterizations of the nonlinear energy transfer for application in wave models. *Journal of Physical Oceanography*, *15*, 1378–1391. https://doi.org/10.1175/1520-0485(1985)015<1378:capotn>2.0.co;2

Hauser, D., Tourain, C., Hermozo, L., Alraddawi, D., Aouf, L., Chapron, B., et al. (2021). New Observations from the SWIM radar on-board CFOSAT: Instrument validation and ocean wave measurement assessment. *IEEE Transactions on Geoscience and Remote Sensing*, *59*, 5. https://doi.org/10.1109/TGRS.2020.2994372

Hell, M. C., Cornelle, B. D., Gille, S. T., Miller, A. J., & Bromirski, P. D. (2019). Identifying ocean swell generation events from Ross Ice Shelf seismic data. *Journal of Atmospheric and Oceanic Technology*, *36*(11), 2171. https://doi.org/10.1175/JTECH-D-19-0093.1

Holthuijsen, L. H., Kuik, A. J., & Mosselman, E. (1987). The response of wave directions to changing wind directions. *Journal of Physical Oceanography*, *17*, 845–853. https://doi.org/10.1175/1520-0485(1987)017<0845:trowdt>2.0.co;2

Hwang, P. A., & Fan, Y. (2017). Effective fetch and duration of tropical cyclone wind fields estimated from simultaneous wind and wave measurements: Surface wave and air-sea exchange computation. *Journal of Physical Oceanography*, *47*, 447–470. https://doi.org/10.1175/JPO-D-16-0180.1

Hwang, P. A., & Walsh, E. J. (2018). Propagation directions of ocean surface waves inside tropical cyclones. *Journal of Physical Oceanography*, *48*(7), 1495–1511. https://doi.org/10.1175/JPO-D-18-0015.1

King, D. B., & Shemdin, O. H. (1978). Radar observations of hurricane wave directions. In *Proceedings of 16th international conference on coastal engineering* (pp. 209–226). American Society of Civil Engineers.
Kitaigorodskii, S. A. (1962). Applications of the theory of similarity to the analysis of wind-generated water waves as a stochastic process. *Bulletin of the Academy of Sciencesof the USSR Geophysics Series*, *1*, 105–117.
Kudryavtsev, V., Golubkin, P., & Chapron, B. (2015). A simplified wave enhancement criterion for moving extreme events. *Journal of Geophysical Research: Oceans*, *120*, 7538–7558. https://doi.org/10.1002/2015JC011284
Kudryavtsev, V., Yurovskaya, M., & Chapron, B. (2021). Self-similarity of surface wave developments under tropical cyclones. *Journal of Geophysical Research: Oceans*, *126*, e2020JC016916. https://doi.org/10.1029/2020JC016916
Kudryavtsev, V., Yurovskaya, M., Chapron, B., Collard, F., & Donlon, C. (2017). Sun glitter imagery of surface waves. Part 2: Waves transformation on ocean currents. *Journal of Geophysical Research: Oceans*, *122*, 1384–1399. https://doi.org/10.1002/2016JC012426
Longuet-Higgins, M. S. (1969). On wavebreaking and the equilibrium spectrum of wind generated waves. *Proceedings of the Royal Society A Mathematical, Physical and Engineering Sciences*, *310*(1501), 151–159. https://doi.org/10.1098/rspa.1969.0069
Merlink, J. F., Makin, V. K., & Kudryavtsev, V. N. (2003). Note on the growth rate of water waves propagating at an arbitrary angle to the wind. *Boundary-Layer Meteorology*, *106*, 171–183. https://doi.org/10.1023/a:1020835211837
Moon, I.-J., Ginis, I., Hara, T., Tolman, H. L., Wright, C. W., & Walsh, E. J. (2003). Numerical simulation of sea surface directional wave spectra under hurricane wind forcing. *Journal of Physical Oceanography*, *33*, 1680–1706. https://doi.org/10.1175/2410.1
Mouche, A., Chapron, B., Knaff, J., Zhao, Y., Zhang, B., & Combot, C. (2019). Copolarized and cross-polarized SAR measurements for high-resolution description of major hurricane wind structures: Application to Irma category 5 hurricane. *Journal of Geophysical Research: Oceans*, *124*, 3905–3922. https://doi.org/10.1029/2019JC015056
Munk, W. H., Miller, G. R., Snodgrass, F. E., & Barber, N. F. (1963). Directional recording of swell from distant storms, *Philosophical Transactions of the Royal Society London, Series A*, *255*, 505–584.
Phillips, O. M. (1977). *The dynamics of the upper ocean* (p. 366). Cambridge University Press.
Phillips, O. M. (1985). Spectral and statistical properties of the equilibrium range in wind-generated gravity waves. *Journal of Fluid Mechanics*, *156*, 505–531. https://doi.org/10.1017/s0022112085002221
Pierson, W. J., Jr, & Moskowitz, L. (1964). A proposed spectral form for fully developed wind seas based on the similarity theory of S. A. Kitaigorodskii. *Journal of Geophysical Research*, *69*, 5181–5190. https://doi.org/10.1029/jz069i024p05181
Plant, W. J. (1982). A relationship between wind stress and wave slope. *Journal of Geophysical Research*, *87*, 1961–1067. https://doi.org/10.1029/jc087ic03p01961
Pushkarev, A., & Zakharov, V. (2015). *On nonlinearity implications and wind forcing in Hasselmann equation*. arXiv:1503.07091 [physics.ao-ph].
Quilfen, Y., Yurovskaya, M., Chapron, B., & Ardhuin, F. (2018). Storm waves focusing and steepening in the Agulhas current: Satellite observations and modeling. *Remote Sensing of Environment*, *216*, 561–571. https://doi.org/10.1016/j.rse.2018.07.020
Reul, N., & Chapron, B. (2003). A model of sea-foam thickness distribution for passive microwave remote sensing applications. *Journal of Geophysical Research*, *108*(C10), 3321. https://doi.org/10.1029/2003JC001887
Reul, N., Chapron, B., Zabolotskikh, E., Donlon, C., Mouche, A., Tenerelli, J., et al. (2017). A new generation of tropical cyclone size measurements from space. *Bulletin of the American Meteorological Society*, *98*, 2367–2385. https://doi.org/10.1175/BAMS-D-15-00291.1
Reul, N., Tenerelli, J., Chapron, B., Vandemark, D., Quilfen, Y., & Kerr, Y. (2012). SMOS satellite L-band radiometer: A new capability for ocean surface remote sensing in hurricanes. *Journal of Geophysical Research*, *117*, C02006. https://doi.org/10.1029/2011JC007474
Snodgrass, F. E., Groves, G. W., Hasselmann, K., Miller, G. R., Munk, W. H., & Powers, W. H. (1966). Propagation of ocean swell across the Pacific. *Philosophical Transactions of the Royal Society of London, Series A*, *249*, 431–497.
Snyder, R. L., Dobson, F. W., Elliott, J. A., & Long, R. B. (1981). Array measurements of atmospheric pressure fluctuations above surface gravity waves. *Journal of Fluid Mechanics*, *102*, 1–59. https://doi.org/10.1017/s0022112081002528
Toba, Y. (1972). Local balance in the air-sea boundary processes. *Journal of the Oceanographical Society of Japan*, *28*, 109–120. https://doi.org/10.1007/BF02109772
Tolman, H. L. (2004). Inverse modeling of discrete interaction approximations for nonlinear interactions in wind waves. *Ocean Modelling*, *6*, 405–422. https://doi.org/10.1016/j.ocemod.2003.09.002
Tolman, H. L. (2009). *User manual and system documentation of WAVEWATCH III version 3.14, Tech. Note 276* (p. 194). NOAA/NWS/NCEP/MMAB.
Tolman, H. L. (2013). A generalized multiple discrete interaction approximation for resonant four-wave interactions in wind wave models. *Ocean Modelling*, *70*, 11–24. https://doi.org/10.1016/j.ocemod.2013.02.005
Tulin, M. (1996). Breaking of ocean waves and downshifting. In Grue, J., Gjevik, B., & Weber, J. E. (Eds.), *Waves and nonlinear processes in hydrodynamics* (p. 177–190). Kluwer Academic Publishers.
van Vledder, G. P., & Holthuijsen, L. H. (1993). The directional response of ocean waves to tuning winds. *Journal of Physical Oceanography*, *23*, 718–728. https://doi.org/10.1175/1520-0485(1993)023<0177:tdroow>2.0.co;2
Wilson, B. W. (1965). Numerical prediction of ocean waves in the North Atlantic for December, 1959. *Deutsche Hydrographische Zeitschrift*, *18*, 114–130. https://doi.org/10.1007/bf02333333
Wright, C. W., Walsh, E. J., Vandemark, D., Krabill, W. B., Garcia, A. W., Houston, S. H., et al. (2001). Hurricane directional wave spectrum spatial variation in the open ocean. *Journal of Physical Oceanography*, *31*, 2472–2488. https://doi.org/10.1175/1520-0485(2001)031<2472:hdwssv>2.0.co;2
Young, I. R. (1988). Parametric Hurricane Wave Prediction Model. *Journal of Waterway, Port, Coastal, and Ocean Engineering*, *114*(5), 637–652. https://doi.org/10.1061/(ASCE)0733-950X(1988)114:5(637)
Young, I. R., Hasselmann, S., & Hasselmann, K. (1987). Computations of the response of a wave spectrum to a sudden change in wind direction. *Journal of Physical Oceanography*, *17*, 1317–1338. https://doi.org/10.1175/1520-0485(1987)017<1317:cotroa>2.0.co;2
Young, I. R., & Vinoth, J. (2013). An "extended fetch" model for the spatial distribution of tropical cyclone wind-waves as observed by altimeter. *Ocean Engineering*, *70*, 14–24. https://doi.org/10.1016/j.oceaneng.2013.05.015
Zakharov, V. E. (2010). Energy balances in a wind-driven sea. *Physica Scripta*, *2010*(T142), 014052. https://doi.org/10.1088/0031-8949/2010/t142/014052